Preprints of the 21st IFAC World Congress (Virtual)
Berlin, Germany, July 12-17, 2020

ESO-based saturated deployment control of tethered satellite system with finite-time tracking performance guarantees ⋆

Caisheng Wei *, **Yanzhu Bian** *, **Yuxin Liao** *, **Shibin Luo** *, **Zeyang Yin** **, **Jianjun Luo** **

* *School of Aeronautics and Astronautics, Central South University, Changsha 410083, China (e-mail:caisheng_wei@csu.edu.cn)*
** *National Key Laboratory of Aerospace Flight Dynamics, Northwestern Polytechnical University, Xi'an 710072, China*

Abstract: This paper investigates a novel finite-time saturated deployment control approach for the tethered satellite system in the presence of uncertain dynamics and space perturbations, as well as state constraints. First, an integral Lyapunov function is constructed to remove the hard state constraints characterized by a finite-time convergent performance function. Then, a backstepping finite-time deployment controller is devised via using an extended state observer (ESO) to approach the unknown dynamics, perturbations and saturation deviation. Compared with the existing finite-time control methods, the prominent advantage of the proposed one is that the finite-time saturated deployment control is achieved without violating the state constraints and using fractional state feedback. Finally, an illustrative example is organized to validate the effectiveness of the proposed approach.

Keywords: Finite-time control, tethered satellite system, saturated control, extended state observer.

1. INTRODUCTION

Space tethered satellite system (TSS) has attracted extensive attention in recent years owing to its potential advantages in debris removal, Earth observation, malfunctioning satellite capture as presented in Misra (2008); He et al. (2011); Yu et al. (2016); Lim and Chung (2018), to just name a few. To guarantee the practical applications, effective deployment control scheme, as a prerequisite, plays a vital role. Thus, various deployment control schemes have sprung up in the existing works. For example, Shi et al. (2017) investigated a sliding mode prediction model control strategy for a three-body TSS consisting of a main satellite and two subsatellites. Zhang and Huang (2019) proposed a novel underactuated controller of the TSS for both on-oribit deployment and retrieval missions. To alleviate the negative effects brought by control saturation, Ma et al. (2017) proposed a dynamic adaptive saturated sliding mode control scheme (SSMC) for a TSS containing a mother satellite and a subsatellite. Moreover, Yu et al. (2017) proposed an analytical tether length rate control law for a flexible TSS via using a simplified elastic rod model with consideration of various space perturbations.

However, there exist two limitations in the aforementioned works. Namely, the first one is that the finite-time convergence rate and tracking accuracy for the TSS cannot be preassigned a priori simultaneously. The second one is that the hard state constraints of the TSS such as the tether tension and length cannot be characterized quantitatively without violation. For the first limitation, in the reported works, sliding mode control (SMC) technique has been widely used to accelerate the deployment convergence rate of the TSS, e.g., see [Kang et al. (2017); Wang and Zhang (2019)] and references therein. Although the finite-time convergence rate can be guaranteed, there are two drawbacks for the SMC-based deployment control schemes. The first one is the complex state-based fractional controller, which is not easily achieved in practice. The second one is the symbolic functions used in the developed controller, which easily renders the control laws discontinuous [Song et al. (2019); Wei et al. (2020)]. To overcome this limitation, in our previous work [Wei et al. (2018b); Yin et al. (2019)], finite-time leader-following consensus control was achieved just via an adjustable time-dependent performance function. Wherein, the finite-time convergence rate and tracking accuracy are guaranteed simultaneously without using fractional state feedback and symbolic function. However, the hard state constraints of the controlled systems are not considered. For the second limitation, the common hard state constraints are easily handled in the constrained optimal control methods like MPC in Mayne (2014). However, deterministic dynamic model is required in the optimization procedure for these control methods. This is not practically effective for the TSS in the presence of uncertain dynamics and complex space perturbations. Thus, it is worth investing how to develop an effective

⋆ This work was supported in part of the Major Program of National Natural Science Foundation of China (Grant No. 61690211), Open Fund of National Key Laboratory of Aerospace Flight Dynamics (Grant No. 6142210200303), Open Fund of Key Laboratory of Space Intelligent Control Technology, and Natural Science Foundation of Hunan Province.

deployment control law for the TSS with consideration of uncertain dynamics and perturbations.

Based on the foregoing observations, this paper investigates a novel finite-time deployment control approach for the TSS subject to uncertain dynamics and perturbations, as well as hard state constraints. Compared with the existing works, twofold contributions are listed as follows: 1) The finite-time convergence rate for the TSS is achieved by removing the hard state constraints based on an integral Lyapunov function. 2) An extended state observer (ESO) is used to compensate the negative effects induced by the uncertain dynamics and perturbations, as well as the control saturation.

The rest of this paper is organized as follows. The dynamic model of the TSS is presented in Section 2. Section 3 shows the detailed design process of the ESO-based saturated deployment controller for the TSS. An illustrative example is organized in Section 4. Some conclusions are drawn in Section 5.

1.1 Notations

T, $|\bullet|$ are the vector transpose and the absolute value of a real number, respectively. $\mathscr{R}^n$, $\mathscr{R}^{n+}$ represent the set of n-dimensional real numbers and n-dimensional positive real numbers, respectively.

2. DYNAMIC MODEL OF THE TETHERED SATELLITE DEPLOYMENT SYSTEM

According to Ma et al. (2017); Wei et al. (2018a), the tethered satellite deployment system can be described by the following equations, i.e.,

$$\begin{aligned}
&\overline{m}\ddot{l}-\overline{m}l\left(\left(\dot{\psi}^2+\left(\dot{\theta}+\omega\right)^2\cos^2\left(\psi\right)\right)+\omega^2\left(3\cos^2\psi\cos^2\theta-1\right)\right)\\
&\qquad=-u_t+d_t\\
&\overline{m}l^2\cos^2\psi\ddot{\theta}+2\overline{m}\left(\dot{\theta}+\omega\right)l^2\cos^2\psi\left(\dot{l}/l-\dot{\psi}\tan\psi\right)+\\
&\qquad3\overline{m}\omega^2l^2\sin\theta\cos\theta\cos^2\psi=u_\theta+d_\theta\\
&\overline{m}l^2\ddot{\psi}+2\overline{m}m\dot{\psi}\dot{l}l+\overline{m}l^2\sin\psi\cos\psi\left(\left(\dot{\theta}+\omega\right)^2+3\omega^2\cos^2\theta\right)\\
&\qquad=u_\psi+d_\psi,
\end{aligned}\tag{1}$$

where m_1 and m_2 are the masses of the mother satellite and subsatellite, respectively. The total mass of the TSS is defined as $m=m_1+m_2$. θ, ψ are, respectively, the roll and pitch angles. The tether length is denoted as l. The in-plane and out-of-plane thruster torques are defined as u_θ and u_ψ, respectively. u_t is the tether tension. The unknown space perturbations are bounded, which are represented by d_t, d_θ, d_ψ, respectively. The orbit angular velocity is defined as ω with $\overline{m}=m_1m_2/m$.

Due to the dimensional differences among the parameters involved in (1), the following transformation is often used to obtain the corresponding dimensionless parameters. Namely, they are

$$\begin{aligned}
&\lambda=l/L,\ \ \mathrm{d}\left(\cdot\right)/\mathrm{d}t=\omega\mathrm{d}\left(\cdot\right)/\mathrm{d}\varpi,\\
&\tau_t=-u_t/\left(\bar{m}\omega^2L\right),\ \ \tau_\theta=u_\theta/\left(\bar{m}\omega^2L^2\right),\\
&\tau_\psi=u_\psi/\left(\bar{m}\omega^2L^2\right),\ \ d_t^*=d_t/\left(\bar{m}\omega^2L\right),\\
&d_\theta^*=d_\theta/\left(\bar{m}\omega^2L^2\right),\ \ d_\psi^*=d_\psi/\left(\bar{m}\omega^2L^2\right),
\end{aligned}\tag{2}$$

where ϖ and L are the true anomaly and reference tethered length, respectively. Then, the dimensionless parameters l, u_t, u_θ, u_ψ, d_t, d_θ, d_ψ are described as λ, τ_t, τ_θ, τ_ψ, d_t, d_θ, d_ψ. Accordingly, a Euler-Lagrange form for the dimensionless system (1) can be obtained as

$$\boldsymbol{\mathcal{M}}\left(\boldsymbol{p}\right)\ddot{\boldsymbol{p}}+\boldsymbol{\mathcal{C}}\left(\boldsymbol{p},\dot{\boldsymbol{p}}\right)\dot{\boldsymbol{p}}+\boldsymbol{\mathcal{G}}\left(\boldsymbol{p}\right)=\boldsymbol{\tau}+\boldsymbol{d}^*,\tag{3}$$

where $\boldsymbol{p}=\left[\lambda,\theta,\psi\right]^T\in\mathscr{R}^3$, $\boldsymbol{\tau}=\left[\tau_1,\tau_2,\tau_3\right]^T=\left[\tau_t,\tau_\theta,\tau_\psi\right]^T\in\mathscr{R}^3$, $\boldsymbol{d}^*=\left[d_t^*,d_\theta^*,d_\psi^*\right]^T\in\mathscr{R}^3$. $\boldsymbol{\mathcal{M}}\left(\boldsymbol{p}\right)$, $\boldsymbol{\mathcal{C}}\left(\boldsymbol{p},\dot{\boldsymbol{p}}\right)$ and $\boldsymbol{\mathcal{G}}\left(\boldsymbol{p}\right)$ are, respectively

$$\boldsymbol{\mathcal{M}}\left(\boldsymbol{p}\right)=\begin{bmatrix}1&0&0\\0&\lambda^2\cos^2\psi&0\\0&0&\lambda^2\end{bmatrix},\boldsymbol{\mathcal{G}}\left(\boldsymbol{p}\right)=\begin{bmatrix}-\lambda\cos^2\psi+\lambda-3\lambda\cos^2\theta\cos^2\psi\\3\lambda^2\cos\theta\sin\theta\cos^2\psi\\\left(1+3\cos^2\theta\right)\lambda^2\sin\psi\cos\psi\end{bmatrix}$$

$$\boldsymbol{\mathcal{C}}\left(\boldsymbol{p},\dot{\boldsymbol{p}}\right)=\begin{bmatrix}0&-(\lambda\dot{\theta}+2\lambda)\cos^2\psi&-\lambda\dot{\psi}\\(2\lambda+\lambda\dot{\theta})\cos^2\psi&\lambda\dot{\lambda}\cos^2\psi-\lambda^2\dot{\psi}\sin\psi\cos\psi&-(\dot{\theta}+2)\lambda^2\sin\psi\cos\psi\\\lambda\dot{\psi}&\lambda^2(\dot{\theta}+2)\sin\psi\cos\psi&\lambda\dot{\lambda}\end{bmatrix}.$$

Remark 1. As presented in (3), one can find that the coriolis and centripetal torque $\boldsymbol{\mathcal{C}}\left(\boldsymbol{p},\dot{\boldsymbol{p}}\right)$ and gravity gradient vector $\boldsymbol{\mathcal{G}}\left(\boldsymbol{p}\right)$ are very complex and difficult to obtain precisely in the corresponding controller design. Thus, it is practically useful when an approximation is developed for such complex nonlinear functions.

In practice, to prevent the collision between the mother satellite and subsatellite, the tether length should satisfy $\lambda\geq\lambda_{\min}>0$ with $\lambda_{\min}$ being a small constant. Moreover, $\lambda\leq\lambda_{\max}$ is to prevent the fracture of the tether with $\lambda_{\max}$ being the maximum tether length ratio. In the meanwhile, the actuator saturation is often encountered. Then, the actuator output $\mathrm{Sat}(\bullet)$ of the TSS is expressed by

$$\mathrm{Sat}(\tau_i)=\begin{cases}\tau_{i,\max},&\tau_i>\tau_{i,\max}\\\tau_i,&\text{otherwise}\\\tau_{i,\min},&\tau_i<\tau_{i,\max}\end{cases},\tag{4}$$

where $\tau_{i,\min}$, $\tau_{i,\max}$ are the relevant lower and upper limitations of τ_i.

For system (3), the control objective of this work is twofold:

(1). The desired reference command for the TSS can be tracked with guaranteed prescribed performance under the devised controller in the presence of unknown space perturbations.

(2). The actuator saturation and asymmetrical tether constraints can be handled well.

3. ESO-BASED SATURATED DEPLOYMENT CONTROLLER DESIGN OF TETHERED SATELLITE SYSTEM

3.1 Performance constraint for the tracking error

To facilitate the corresponding controller design, by defining $\boldsymbol{q}_1=\boldsymbol{p}$, $\boldsymbol{q}_2=\dot{\boldsymbol{p}}$, an equivalent strict-feedback form of system (3) is obtained as

$$\begin{cases}\dot{\boldsymbol{q}}_1=\boldsymbol{q}_2\\\dot{\boldsymbol{q}}_2=\boldsymbol{f}_1\left(\boldsymbol{q}_1,\boldsymbol{q}_2\right)+\boldsymbol{\mathcal{M}}^{-1}\left(\boldsymbol{q}_1\right)\mathrm{Sat}\left(\boldsymbol{\tau}\right)+\overline{\boldsymbol{d}}\end{cases},\tag{5}$$

where $\boldsymbol{f}_1\left(\boldsymbol{q}_1,\boldsymbol{q}_2\right)=-\boldsymbol{\mathcal{M}}^{-1}\left(\boldsymbol{q}_1\right)\left[\boldsymbol{\mathcal{C}}\left(\boldsymbol{q}_1,\boldsymbol{q}_2\right)\boldsymbol{q}_2+\boldsymbol{\mathcal{G}}\left(\boldsymbol{q}_1\right)\right]$. To achieve the control objective, we define the desired

reference command as $\boldsymbol{q}_r$. Then, the tracking error vector for system (5) is expressed by $\boldsymbol{e}_1 = [e_{1,1}, e_{1,2}, e_{1,3}]^T = \boldsymbol{q}_1 - \boldsymbol{q}_r$. To handle the physical state constraints (like the tether length constraint) and quantitatively characterize the tracking performance, based on the work done by Bechlioulis and Rovithakis (2008), the following unsymmetrical constraint is imposed on the tracking error vector, i.e.,

$$-\delta_{1,i}\rho_i(t) < e_{1,i} < \delta_{2,i}\rho_i(t) \ (i = 1, 2, 3), \tag{6}$$

where $\delta_{1,i}$, $\delta_{2,i}$ are non-negative constants. $\rho_i(t)$ is the performance function, which satisfies $\rho_i(t) > 0$. To simplify the relevant design procedure, all the performance function is devised as a same one. In this case, the subscript of $\rho(t)$ can be removed for brevity, namely, $\rho(t) = \rho_i(t)$. The performance function $\rho(t)$ is derived by the following differential equation

$$\dot{\rho}(t) = \begin{cases} -\ell_0(\rho(t) - \rho_\infty)^\vartheta, & \text{if } t \le t_f \\ 0, & \text{otherwise} \end{cases}, \tag{7}$$

where the initial state $\rho(0)$ satisfies $\rho(0) = \rho_0 > \rho_\infty > 0$ with ρ_0, ρ_∞ being positive constants. t_f is the appointed convergent time. The rest parameters in (7) are design constants, which are defined as $\vartheta \in (0, 1)$, $\ell_0 = \left((\rho_0 - \rho_\infty)^{1-\vartheta}\right) / ((1-\vartheta) t_f)$. For performance function $\rho(t)$, the following lemma is derived.

Lemma 1. Performance function $\rho(t)$ will converge to ρ_∞ at the appointed time T. When $t \ge T$, performance function $\rho(t)$ will keep invariable, i.e., $\rho(t) = \rho_\infty$ Proof. To prove Lemma 1, based on the authors' previous work in Wei et al. (2018b), the following Lyapunov function V_ρ is devised

$$V_\rho = \frac{1}{2}(\rho(t) - \rho_\infty)^2. \tag{8}$$

Based on (7), the derivative of V_ρ is

$$\begin{aligned} \dot{V}_\rho &= (\rho(t) - \rho_\infty)\dot{\rho}(t) \\ &= -\ell_0(\rho(t) - \rho_\infty)^{\vartheta+1} \\ &= -2^{\frac{\vartheta+1}{2}}\ell_0 V_\rho^{\frac{\vartheta+1}{2}}. \end{aligned} \tag{9}$$

According to Wei et al. (2018b), the relevant convergence time for $\rho(t) - \rho_\infty$ satisfies

$$\begin{aligned} t &\le \frac{1}{2^{\frac{\vartheta+1}{2}}\ell_0\left(1 - \frac{\vartheta+1}{2}\right)} V_\rho^{1-\frac{\vartheta+1}{2}}(0) \\ &= \frac{1}{2^{\frac{\vartheta+1}{2}}\frac{(\rho_0-\rho_\infty)^{1-\vartheta}}{(1-\vartheta)T}(1-\vartheta)} 2^{\frac{\vartheta+1}{2}}(\rho_0 - \rho_\infty)^{1-\vartheta} \\ &= t_f. \end{aligned} \tag{10}$$

Accordingly, one can obtain that $\rho(t) - \rho_\infty$ will converge to zero at the appointed time t_f. Namely, $\rho(t)$ will converge to ρ_∞ within the appointed time t_f. As presented in (7), when $t \ge t_f$, $\rho(t)$ will keep constant, i.e., $\rho(t) = \rho_\infty$ $\forall t \ge t_f$. Then, the proof of Lemma 1 is finished. ■

Remark 2. As the proof of Lemma 1 shows, when parameter $\rho_\infty \to zero$, one can find that the tracking error will converge to zero around the appointed time t_f. In the meanwhile, the transient and steady-state tracking performance can be preassigned by the designed performance function $\rho(t)$. In this sense, the finite-time or fixed-time convergence rate and tracking performance can be guaranteed simultaneously. This is different from the traditional finite-time control methods like in Yu and Long (2015); Wang and Zhang (2019), wherein, only the finite-time convergence rate can be guaranteed.

3.2 ESO-based saturated deployment controller design

Based on the foregoing analysis, the ESO-based saturated deployment controller is devised as follows. In this part, according to Freeman and Kokotović (1993), baskstepping technique is used to facilitate the relevant controller design for system (5), wherein, two steps are involved. Without inducing ambiguity, (t) in the performance function $\rho(t)$ is removed for brevity henceforth.

Step 1. To guarantee the predefined tracking performance, the following integral function is designed

$$\begin{aligned} V_1 = \sum_{i=1}^{3} \Bigg[&(1 - \varrho(e_{1,i})) \int_0^{e_{1,i}} \frac{x\delta_{1,i}^2\rho^2}{\delta_{1,i}^2\rho^2 - x^2}\mathrm{d}x + \\ &\varrho(e_{1,i}) \int_0^{e_{1,i}} \frac{x\delta_{2,i}^2\rho^2}{\delta_{2,i}^2\rho^2 - x^2}\mathrm{d}x \Bigg], \end{aligned} \tag{11}$$

where $\varrho(\bullet) = \begin{cases} 1, & \text{if } \bullet \ge 0 \\ 0, & \text{otherwise} \end{cases}$. For the involved terms of (11), one can obtain that $\int_0^{e_{1,i}} \frac{x\delta_{j,i}^2\rho^2}{\delta_{j,i}^2\rho^2 - x^2}\mathrm{d}x = -\frac{1}{2}\ln\left(\delta_{j,i}^2\rho^2 - x^2\right)\Big|_0^{e_{1,i}} = \frac{1}{2}\ln\frac{\delta_{j,i}^2\rho^2}{\delta_{j,i}^2\rho^2 - e_{1,i}^2} \ge 0$ in the presence of $-\delta_{1,i}\rho < e_{1,i} < \delta_{2,i}\rho$ $(j = 1, 2,\ i = 1, 2, 3)$. Moreover, function V_1 is derivable. So V_1 in (11) can be chosen as a Lyapunov function. Taking the time-derivative of V_1 yields

$$\begin{aligned} \dot{V}_1 = \sum_{i=1}^{3} \Bigg[&(1 - \varrho(e_{1,i})) \frac{\delta_{1,i}^2\rho^2 e_{1,i}}{\delta_{1,i}^2\rho^2 - e_{1,i}^2}\dot{e}_{1,i} \\ &- (1 - \varrho(e_{1,i})) \int_0^{e_{1,i}} \frac{2x^3\delta_{1,i}^2\rho\dot{\rho}}{\left(\delta_{1,i}^2\rho^2 - x^2\right)^2}\mathrm{d}x \\ &+ \varrho(e_{1,i}) \frac{\delta_{2,i}^2\rho^2 e_{1,i}}{\delta_{2,i}^2\rho^2 - e_{1,i}^2}\dot{e}_{1,i} \\ &- \varrho(e_{1,i}) \int_0^{e_{1,i}} \frac{2x^3\delta_{2,i}^2\rho\dot{\rho}}{\left(\delta_{2,i}^2\rho^2 - x^2\right)^2}\mathrm{d}x \Bigg] \\ = \sum_{i=1}^{3} &(\gamma_i\dot{e}_{1,i} + \eta_i), \end{aligned} \tag{12}$$

where $\gamma_i = (1 - \varrho(e_{1,i}))\frac{\delta_{1,i}^2\rho^2 e_{1,i}}{\delta_{1,i}^2\rho^2 - e_{1,i}^2} + \varrho(e_{1,i})\frac{\delta_{2,i}^2\rho^2 e_{1,i}}{\delta_{2,i}^2\rho^2 - e_{1,i}^2}$, $\eta_i = -(1 - \varrho(e_{1,i}))\int_0^{e_{1,i}} \frac{2x^3\delta_{1,i}^2\rho\dot{\rho}}{\left(\delta_{1,i}^2\rho^2 - x^2\right)^2}\mathrm{d}x$ $-\varrho(e_{1,i})\int_0^{e_{1,i}} \frac{2x^3\delta_{2,i}^2\rho\dot{\rho}}{\left(\delta_{2,i}^2\rho^2 - x^2\right)^2}\mathrm{d}x$. Based on the tracking error vector $\boldsymbol{e}_1$ of the TSS defined in (6), one can obtain that $\dot{e}_{1,i} = \dot{q}_{1,i} - \dot{q}_{r,i} = q_{2,i} - \dot{q}_{r,i}$ $(i = 1, 2, 3)$. To develop the relevant controller, the second tracking error vector $\boldsymbol{e}_2$ is defined, i.e., $\boldsymbol{e}_2 = \boldsymbol{q}_2 - \boldsymbol{\chi}_1$ with $\boldsymbol{\chi}_1 = [\chi_{1,1}, \chi_{1,2}, \chi_{1,3}]^T$ being the output of a first-order filter. Wherein, the first-order filter is used to avoid taking the complex time derivative of the virtual controller. In detail, the ith element of $\boldsymbol{\chi}_1$ is obtained as

$$\varepsilon_{0,i}\dot{\chi}_{1,i} = \alpha_{1,i} - \chi_{1,i},\ \chi_{1,i}(0) = \alpha_{1,i}(0), \tag{13}$$

where $\alpha_{1,i}$ is the ith element of virtual controller $\boldsymbol{\alpha}_1$, which is devised later. Then, we define the filter error $\varsigma_{0,i}$ as

$\varsigma_{0,i} = \alpha_{1,i} - \chi_{1,i}$. Accordingly, $q_{2,i} = e_{2,i} + \alpha_{1,i} - \varsigma_{0,i}$. Substituting $q_{2,i}$ into (12) leads to

$$\dot{V}_1 = \sum_{i=1}^{3} \left(\gamma_i \dot{e}_{1,i} + \eta_i\right) = \sum_{i=1}^{3} \left(\gamma_i \left(e_{2,i} + \alpha_{1,i} - \varsigma_{0,i}\right) + \eta_i\right). \tag{14}$$

With consideration of $\gamma_i = \left(1 - \varrho\left(e_{1,i}\right)\right) \frac{\delta_{1,i}^2 \rho^2 e_{1,i}}{\delta_{1,i}^2 \rho^2 - e_{1,i}^2} + \varrho\left(e_{1,i}\right) \frac{\delta_{2,i}^2 \rho^2 e_{1,i}}{\delta_{2,i}^2 \rho^2 - e_{1,i}^2}$, applying the Young's inequality yields

$$\begin{aligned} \gamma_i e_{2,i} \leq & \left(1 - \varrho\left(e_{1,i}\right)\right) \frac{\delta_{1,i}^4 \rho^4 e_{1,i}^2}{\left(\delta_{1,i}^2 \rho^2 - e_{1,i}^2\right)^2} \\ & + \varrho\left(e_{1,i}\right) \frac{\delta_{2,i}^4 \rho^4 e_{1,i}^2}{\left(\delta_{2,i}^2 \rho^2 - e_{1,i}^2\right)^2} + \frac{1}{2} e_{2,i}^2 \\ -\gamma_i \varsigma_{0,i} \leq & \left(1 - \varrho\left(e_{1,i}\right)\right) \frac{\delta_{1,i}^4 \rho^4 e_{1,i}^2}{\left(\delta_{1,i}^2 \rho^2 - e_{1,i}^2\right)^2} \\ & + \varrho\left(e_{1,i}\right) \frac{\delta_{2,i}^4 \rho^4 e_{1,i}^2}{\left(\delta_{2,i}^2 \rho^2 - e_{1,i}^2\right)^2} + \frac{1}{2} \varsigma_{0,i}^2. \end{aligned} \tag{15}$$

Based on (15), one can obtain

$$\begin{aligned} \gamma_i \left(e_{2,i} - \varsigma_{0,i}\right) \leq & \left(1 - \varrho\left(e_{1,i}\right)\right) \frac{2\delta_{1,i}^4 \rho^4 e_{1,i}^2}{\left(\delta_{1,i}^2 \rho^2 - e_{1,i}^2\right)^2} \\ & + \varrho\left(e_{1,i}\right) \frac{2\delta_{2,i}^4 \rho^4 e_{1,i}^2}{\left(\delta_{2,i}^2 \rho^2 - e_{1,i}^2\right)^2} + \frac{1}{2}\left(e_{2,i}^2 + \varsigma_{0,i}^2\right). \end{aligned} \tag{16}$$

Then, the first virtual controller $\alpha_{1,i}$ $(i = 1, 2, 3)$ is devised as

$$\begin{aligned} \alpha_{1,i} = & -k_{1,i} e_{1,i} + \dot{q}_{r,i} - \left(1 - \varrho\left(e_{1,i}\right)\right) \frac{2\delta_{1,i}^2 \rho^2 e_{1,i}}{\delta_{1,i}^2 \rho^2 - e_{1,i}^2} \\ & - \varrho\left(e_{1,i}\right) \frac{2\delta_{2,i}^2 \rho^2 e_{1,i}}{\delta_{2,i}^2 \rho^2 - e_{1,i}^2} - \frac{\eta_i}{\gamma_i}, \end{aligned} \tag{17}$$

where $k_{1,i}$ is a positive control gain. Note that for term $\frac{\eta_i}{\gamma_i}$, there exists $\lim_{e_{1,i} \to 0} \frac{\eta_i}{\gamma_i} = 0$ based on (12). Note that the time-derivative of virtual controller $\alpha_{1,i}$ is difficult to calculate. Thus, the first-order filter in (13) is used to approximate the time-derivative of the virtual controller, which will be used in the actual controller design later. Substituting (16) and (17) into (14) gets

$$\begin{aligned} \dot{V}_1 \leq & -\sum_{i=1}^{3} k_{1,i} \rho^2 e_{1,i}^2 \left(\left(1 - \varrho\left(e_{1,i}\right)\right) \frac{\delta_{1,i}^2}{\delta_{1,i}^2 \rho^2 - e_{1,i}^2} \right. \\ & \left. - \varrho\left(e_{1,i}\right) \frac{\delta_{2,i}^2}{\delta_{2,i}^2 \rho^2 - e_{1,i}^2} \right) + \frac{1}{2} \sum_{i=1}^{3} \left(e_{2,i}^2 + \varsigma_{0,i}^2\right). \end{aligned} \tag{18}$$

Step 2. With consideration of $\boldsymbol{e}_2 = \boldsymbol{q}_2 - \boldsymbol{\chi}_1$, based on (5), the time-derivative of $\boldsymbol{e}_2$ is

$$\begin{aligned} \dot{\boldsymbol{e}}_2 &= \dot{\boldsymbol{q}}_2 - \dot{\boldsymbol{\chi}}_1 \\ &= \boldsymbol{f}_1\left(\boldsymbol{q}_1, \boldsymbol{q}_2\right) + \boldsymbol{\mathcal{M}}^{-1}\left(\boldsymbol{q}_1\right) \mathrm{Sat}\left(\boldsymbol{\tau}\right) + \overline{\boldsymbol{d}} - \dot{\boldsymbol{\chi}}_1 \\ &= \boldsymbol{f}_1\left(\boldsymbol{q}_1, \boldsymbol{q}_2\right) + \boldsymbol{\mathcal{M}}^{-1}\left(\boldsymbol{q}_1\right) \left(\mathrm{Sat}\left(\boldsymbol{\tau}\right) - \boldsymbol{\tau} + \boldsymbol{\tau}\right) + \overline{\boldsymbol{d}} - \dot{\boldsymbol{\chi}}_1 \\ &= \boldsymbol{f}_1^*\left(\boldsymbol{q}_1, \boldsymbol{q}_2, \overline{\boldsymbol{d}}\right) + \boldsymbol{\mathcal{M}}^{-1}\left(\boldsymbol{q}_1\right) \boldsymbol{\tau} - \dot{\boldsymbol{\chi}}_1, \end{aligned} \tag{19}$$

where $\boldsymbol{f}_1^*\left(\boldsymbol{q}_1, \boldsymbol{q}_2, \overline{\boldsymbol{d}}\right) = \boldsymbol{f}_1\left(\boldsymbol{q}_1, \boldsymbol{q}_2\right) + \boldsymbol{\mathcal{M}}^{-1}\left(\boldsymbol{q}_1\right)\left(\mathrm{Sat}\left(\boldsymbol{\tau}\right) - \tau\right) + \overline{\boldsymbol{d}}$ is an unknown lumped nonlinear function, which is estimated by a ESO. Namely, based on Yang et al. (2018), its detailed form is expressed by

$$\begin{cases} \dot{z}_{1,i} = z_{2,i} - \mu_{1,i}\left(z_{1,i} - e_{2,i}\right) + \bar{\tau}_i - \dot{\chi}_{1,i} \\ \dot{z}_{2,i} = -\mu_{2,i} |z_{1,i} - e_{2,i}|^{\kappa_i} \mathrm{sign}\left(z_{1,i} - e_{2,i}\right) \end{cases}, \tag{20}$$

where $\overline{\boldsymbol{\tau}} = [\overline{\tau}_1, \overline{\tau}_2, \overline{\tau}_3]^T = \boldsymbol{\mathcal{M}}^{-1}\left(q_1\right) \boldsymbol{\tau}$, $\mu_{1,i}, \mu_{2,i} > 0$, $\kappa_i \in (0,1)$ $(i = 1, 2, 3)$ are relevant design constants.

According to Huang and Han (2000), there exist ESO gains $\mu_{1,i}, \mu_{2,i} > 0$, $\kappa_i \in (0,1)$ such as $z_{1,i}$ and $z_{2,i}$ converge to $e_{2,i}$ and function $\boldsymbol{f}_{1,i}*$. The detailed proof can be found in Huang and Han (2000), which is omitted for brevity. Based on the foregoing analysis, one important conclusion is stated in the following theorem.

Theorem 1. The prescribed performance for the TSS in (6) can be achieved within the appointed time t_f under the following devised actual controller.

$$\boldsymbol{\tau} = \boldsymbol{\mathcal{M}}\left(\boldsymbol{q}_1\right)\left(-\boldsymbol{k}_2 \boldsymbol{e}_2 - \boldsymbol{e}_2 - \boldsymbol{z}_2 + \dot{\boldsymbol{\chi}}_1\right), \tag{21}$$

where $\boldsymbol{k}_2 = \mathrm{diag}\left\{k_{2,1}, k_{2,2}, k_{2,3}\right\}$ is a diagonal positive-definite control gain. In the meanwhile, all the involved states are uniformly ultimately bounded.

Proof. To prove Theorem 1, the following Lyapunov function is chosen as

$$V_2 = V_1 + \frac{1}{2} \boldsymbol{e}_2^T \boldsymbol{e}_2. \tag{22}$$

Based on (19), the time-derivative of V_2 is

$$\begin{aligned} \dot{V}_2 &= \dot{V}_1 + \boldsymbol{e}_2^T \dot{\boldsymbol{e}}_2 = \boldsymbol{e}_2^T \left(\dot{\boldsymbol{q}}_2 - \dot{\boldsymbol{\chi}}_1\right) \\ &= \boldsymbol{e}_2^T \left(\boldsymbol{f}_1^*\left(\boldsymbol{q}_1, \boldsymbol{q}_2, \overline{\boldsymbol{d}}\right) + \boldsymbol{\mathcal{M}}^{-1}\left(\boldsymbol{q}_1\right) \boldsymbol{\tau} - \dot{\boldsymbol{\chi}}_1\right). \end{aligned} \tag{23}$$

By substituting (18) and (21) into (23), one can obtain

$$\begin{aligned} \dot{V}_2 \leq & -\sum_{i=1}^{3} k_{1,i} \rho^2 e_{1,i}^2 \left(\left(1 - \varrho\left(e_{1,i}\right)\right) \frac{\delta_{1,i}^2}{\delta_{1,i}^2 \rho^2 - e_{1,i}^2} \right. \\ & \left. - \varrho\left(e_{1,i}\right) \frac{\delta_{2,i}^2}{\delta_{2,i}^2 \rho^2 - e_{1,i}^2} \right) + \frac{1}{2} \sum_{i=1}^{3} \left(e_{2,i}^2 + \varsigma_{0,i}^2\right) \\ & - \boldsymbol{k}_2 \boldsymbol{e}_2^T \boldsymbol{e}_2 - \boldsymbol{e}_2^T \boldsymbol{e}_2 + \boldsymbol{e}_2^T \left(\boldsymbol{f}_1^*\left(\boldsymbol{q}_1, \boldsymbol{q}_2, \overline{\boldsymbol{d}}\right) - \boldsymbol{z}_2\right). \end{aligned} \tag{24}$$

Define the ESO-based approximation error $\hbar_0 = [\hbar_{0,1}, \hbar_{0,2}, \hbar_{0,3}] = \boldsymbol{f}_1^*\left(\boldsymbol{q}_1, \boldsymbol{q}_2, \overline{\boldsymbol{d}}\right) - \boldsymbol{z}_2$. According to Huang and Han (2000), the approximation error $\hbar_0$ can be made sufficiently small. So it is bounded.

By using Young's inequality, (24) becomes

$$\begin{aligned} \dot{V}_2 \leq & -\sum_{i=1}^{3} k_{1,i} \rho^2 e_{1,i}^2 \left(\left(1 - \varrho\left(e_{1,i}\right)\right) \frac{\delta_{1,i}^2}{\delta_{1,i}^2 \rho^2 - e_{1,i}^2} \right. \\ & \left. - \varrho\left(e_{1,i}\right) \frac{\delta_{2,i}^2}{\delta_{2,i}^2 \rho^2 - e_{1,i}^2} \right) - \boldsymbol{k}_2 \boldsymbol{e}_2^T \boldsymbol{e}_2 + \frac{1}{2} \sum_{i=1}^{3} \left(\hbar_{0,i}^2 + \varsigma_{0,i}^2\right). \end{aligned} \tag{25}$$

In light of (25), one can find that the tracking errors $\boldsymbol{e}_1$ and $\boldsymbol{e}_2$ of the TSS are uniformly ultimately bounded. Thus, the preassigned tracking performance in (6) can be achieved under the devised controller. This completes the proof of Theorem 1. ■

4. ILLUSTRATIVE SIMULATIONS

To demonstrate the effectiveness of the proposed control approach, the following numerical example is organized. Wherein, without loss of generality, the desired reference

command $\boldsymbol{q}_r$ is chosen as $[1,0,0]^T$ based on Wei et al. (2018a). The relevant simulation parameters are listed in Table 1. The initial states $z_{1,i}$ and $z_{2,i}$ of the ESO are set as 0 ($i = 1,2,3$). The lower saturation bound for the control torque is $[-5,-5,-5]^T$. The saturation bound is $[0,-5,5]^T$. The initial dimensionless state vectors $\boldsymbol{q}_1$ and $\boldsymbol{q}_2$ are set as $[0.3,-0.5,0.5]^T$ and $[0,0,0]^T$, respectively. The lumped space perturbation vector $\boldsymbol{d}^*$ is chosen as the set as that in Wei et al. (2018a). To highlight the advantages of our proposed control approach, simulation results with the SSMC method and Proportional-Differential (PD) control method work as the comparative tests based on Ma et al. (2017) and Wei et al. (2018a). The demonstrative simulation results are shown in Figs. 1–6.

Table 1. Values of the simulation parameters

Equations	Values of the design parameters
(6)	$\delta_{1,1} = \delta_{1,2} = \delta_{1,3} = 1$
	$\delta_{2,1} = 10^{-5},\ \delta_{2,2} = \delta_{2,3} = 1$
(7)	$\vartheta = 0.2,\ \rho_0 = 1,\ \rho_\infty = 0.05,\ t_f = 3$
(13)	$\varepsilon_{0,1} = 0.001,\ \varepsilon_{0,2} = \varepsilon_{0,3} = 0.002$
(17)	$k_{1,1} = 1.7,\ k_{1,2} = 4,\ k_{1,3} = 2$
(20)	$\mu_{1,1} = \mu_{1,2} = \mu_{1,3} = 5$
	$\mu_{1,1} = \mu_{1,2} = \mu_{1,3} = 10$
	$\kappa_1 = \kappa_2 = \kappa_3 = 0.5$
(21)	$k_{2,1} = 60,\ k_{1,2} = k_{1,3} = 5$

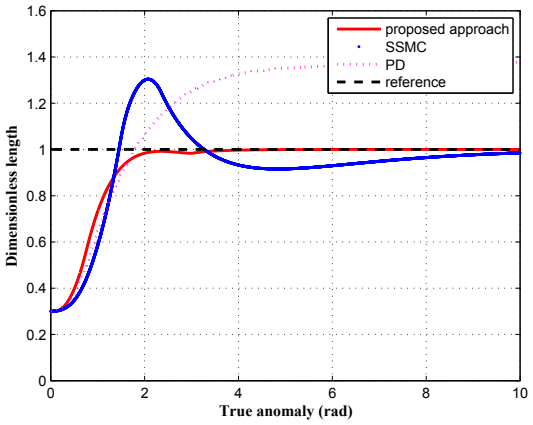

Fig. 1. Time response of dimensionless length

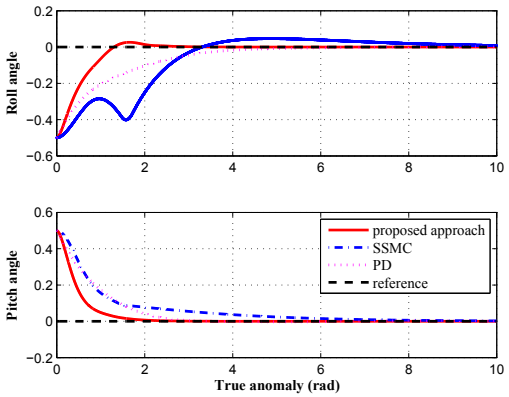

Fig. 2. Time responses of in-plane and out-of-plane angles

Portrayed from these figures, one can conclude that: 1) Figure 1 presents that the physical hard constraint for the tether length is not violated under the proposed approach. However, under the SSMC and PD control methods, the tether is easily fractured due to the fact that the longest tether length is more than 1. In the meanwhile, the convergent rate is fastest and the tracking accuracy is the highest among the three control methods (as Figs. 1 and 2 illustrates). This is because that the finite-time or appointed-time convergence rate can be prescribed a priori. 2) Figure 3 shows that the transient and steady-state tracking performance for the TSS can be guaranteed in the whole time domain. 3) In Figs. 4–6, one can find that there exists serious chattering phenomenon in the SSMC

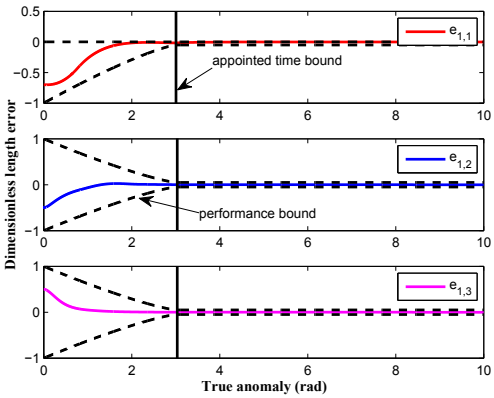

Fig. 3. Prescribed performance for the tracking errors

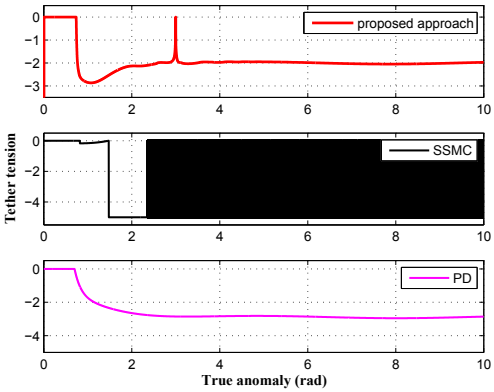

Fig. 4. Time response of the tether tension

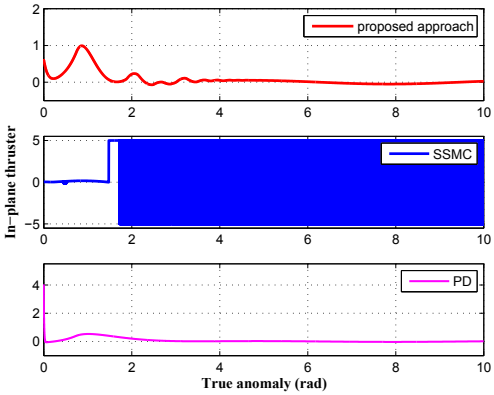

Fig. 5. Time response of the in-plane thrust

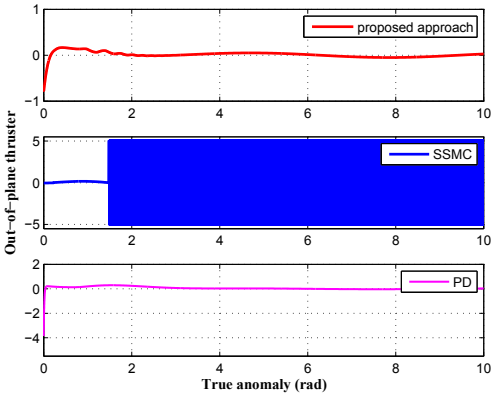

Fig. 6. Time response of the out-of-plane thrust

method, which is an inherent drawback of the SMC-based control methods. This demonstrates that a compensation control input (like the periodic jump of the control input between zero and -5 in Fig. 4)is required for the time-varying space perturbations as presented in [Wei et al. (2018a)]

While, the control torque is comparative smooth under the proposed controller and PD controller.

To be brief, the illustrative simulations show that the proposed control approach has prominent advantages in preassigning the convergence rate and tracking accuracy.

5. CONCLUSION

A saturated finite-time or appointed-time deployment control approach has been proposed for the tether satellite system with consideration of space perturbations. Wherein, an integral Lyapunov function is built to remove the hard state constraints quantitatively characterized by a performance function. Moreover, an extended state observer is used to compensate the negative effects brought by the uncertain dynamics and perturbations, as well as the saturation. The illustrative example shows that faster convergence rate and higher tracking accuracy can be achieved without any violation for the hard state constraints compared with the saturated sliding mode control and PD control methods.

REFERENCES

Bechlioulis, C.P. and Rovithakis, G.A. (2008). Robust adaptive control of feedback linearizable mimo nonlinear systems with prescribed performance. IEEE Transactions on Automatic Control, 53(9), 2090–2099.

Freeman, R. and Kokotović, P. (1993). Backstepping design of robust controllers for a class of nonlinear systems. In Nonlinear Control Systems Design 1992, 431–436. Elsevier.

He, Y., Liang, B., and Xu, W. (2011). Study on the stability of tethered satellite system. Acta Astronautica, 68(11-12), 1964–1972.

Huang, Y. and Han, J. (2000). Analysis and design for the second order nonlinear continuous extended states observer. Science Bulletin.

Kang, J., Zhu, Z.H., Wang, W., Li, A., and Wang, C. (2017). Fractional order sliding mode control for tethered satellite deployment with disturbances. Advances in Space Research, 59(1), 263–273.

Lim, J. and Chung, J. (2018). Dynamic analysis of a tethered satellite system for space debris capture. Nonlinear Dynamics, 94(4), 2391–2408.

Ma, Z., Sun, G., and Li, Z. (2017). Dynamic adaptive saturated sliding mode control for deployment of tethered satellite system. Aerospace Science and Technology, 66, 355–365.

Mayne, D.Q. (2014). Model predictive control: Recent developments and future promise. Automatica, 50(12), 2967–2986.

Misra, A. (2008). Dynamics and control of tethered satellite systems. Acta Astronautica, 63(11-12), 1169–1177.

Shi, G., Zhu, Z., Chen, S., Yuan, J., and Tang, B. (2017). The motion and control of a complex three-body space tethered system. Advances in Space Research, 60(10), 2133–2145.

Song, Y., Wang, Y., and Krstic, M. (2019). Time-varying feedback for stabilization in prescribed finite time. International Journal of Robust and Nonlinear Control, 29(3), 618–633.

Wang, C. and Zhang, F. (2019). Finite-time stability of an underactuated tethered satellite system. Acta Astronautica, 159, 199–212.

Wei, C., Liao, Y., Xi, W., Yin, Z., and Luo, J. (2020). Event-driven adaptive fault-tolerant tracking control for uncertain mechanical systems with application to flexible spacecraft. Journal of Vibration and Control, 1077546320902562.

Wei, C., Luo, J., Gong, B., Wang, M., and Yuan, J. (2018a). On novel adaptive saturated deployment control of tethered satellite system with guaranteed output tracking prescribed performance. Aerospace Science and Technology, 75, 58–73.

Wei, C., Luo, J., Yin, Z., and Yuan, J. (2018b). Leader-following consensus of second-order multi-agent systems with arbitrarily appointed-time prescribed performance. IET Control Theory & Applications, 12(16), 2276–2286.

Yang, Y., Tan, J., and Yue, D. (2018). Prescribed performance tracking control of a class of uncertain pure-feedback nonlinear systems with input saturation. IEEE Transactions on Systems, Man, and Cybernetics: Systems, to be publised, doi: 10.1109/TSMC.2017.2784451.

Yin, Z., Luo, J., and Wei, C. (2019). Quasi fixed-time fault-tolerant control for nonlinear mechanical systems with enhanced performance. Applied Mathematics and Computation, 352, 157–173.

Yu, B., Jin, D., and Wen, H. (2016). Nonlinear dynamics of flexible tethered satellite system subject to space environment. Applied Mathematics and Mechanics, 37(4), 485–500.

Yu, B., Jin, D., and Wen, H. (2017). Analytical deployment control law for a flexible tethered satellite system. Aerospace Science and Technology, 66, 294–303.

Yu, S. and Long, X. (2015). Finite-time consensus for second-order multi-agent systems with disturbances by integral sliding mode. Automatica, 54, 158–165.

Zhang, F. and Huang, P. (2019). A novel underactuated control scheme for deployment/retrieval of space tethered system. Nonlinear Dynamics, 95(4), 3465–3476.